ACCSCIENCE PUBLISHING

International Journal of Bioprinting

RESEARCH ARTICLE

3D bioprinting of biomimetic trachea with interspersed cartilage and vascularized connective tissue for prompt segmental tracheal reconstruction

Pengli Wang[1†], Ziming Wang[1†], Bohui Li[2], Lei Xie[3], Liang Guo[1], Yong Xu[1*], Dan Li[4*], Jiaoyu Yi[5*], and Bo Tao[1*]

[1]Department of Thoracic Surgery, Shanghai Pulmonary Hospital, School of Medicine, Tongji University, Shanghai, China

[2]Plastic Surgery Institute, Shandong Second Medical University, Weifang, Shandong, China

[3]Department of Thoracic Surgery, The Second Affiliated Hospital of Nanchang University, Nanchang, Jiangxi, China

[4]Department of Plastic and Reconstructive Surgery, Shanghai 9th People's Hospital, Shanghai Jiao Tong University School of Medicine, Shanghai, China.

[5]Department of Plastic Surgery, Renji Hospital, Shanghai Jiaotong University School of Medicine, Shanghai, China

(This article belongs to the *Special Issue: Bioprinting of Tissues and Organs: Materials, Technologies and Perspectives for Regenerative Medicine*)

Abstract

Segmental tracheal reconstruction remains a significant clinical challenge due to the lack of ideal tracheal substitutes. Three-dimensional (3D) bioprinting technique offers a promising avenue for the development of native-like tracheal substitutes. However, several challenges remain to be addressed, including deformation of 3D-printed C-shaped cell-laden hydrogels, fusion of regenerated C-shaped cartilage, and difficulty in regenerating vascularized connective tissue. Herein, we utilized 3D printing techniques to fabricate C-shaped chondrocyte-laden GelMA/PCL (CcGP) and S-shaped PCL chains (SPC). These were assembled into the SPC-CcGP construct, followed by mold casting (VEGF@GelMA) to establish tissue-engineered tracheal construct (TETC). *In vitro* experiments confirmed the stable chondrogenic potential of CcGP and the angiogenic capability of VEGF@GelMA. Subcutaneous implantation in nude mice and orthotopic transplantation in rabbit model further demonstrated that the TETC could achieve stable regeneration of cartilage and vascularized connective tissue. The engineered trachea could maintain luminal patency following prompt repair of rabbit tracheal defects. This study offers a promising approach for developing engineered tracheas with regenerated cartilage and vascularized connective tissue for prompt and effective segmental tracheal defect repair.

Keywords: 3D printing; Mold; Cartilage; Trachea reconstruction; Vascularized connective tissue

[†]These authors contributed equally to this work.

***Corresponding authors:**
Yong Xu (xuyong@tongji.edu.cn)
Dan Li (lidan2009best@163.com)
Jiaoyu Yi (yijiaoyu@renji.com)
Bo Tao (tbo0820@163.com)

Citation: Wang P, Wang Z, Li B, et al. 3D bioprinting of biomimetic trachea with interspersed cartilage and vascularized connective tissue for prompt segmental tracheal reconstruction. *Int J Bioprint*. 2025;11(1):314-326. doi: 10.36922/ijb.4955

Received: September 25, 2024
Revised: November 3, 2024
Accepted: November 19, 2024
Published Online: November 20, 2024

Copyright: © 2024 Author(s). This is an Open Access article distributed under the terms of the Creative Commons Attribution License, permitting distribution, and reproduction in any medium, provided the original work is properly cited.

Publisher's Note: AccScience Publishing remains neutral with regard to jurisdictional claims in published maps and institutional affiliations.

1. Introduction

Tissue engineered tracheal constructs (TETC) present a promising approach for the reconstruction of long-segment tracheal defects in which end-to-end anastomosis is not viable.[1] The trachea is a C-shaped cartilaginous tubular structure connecting the larynx superiorly and the main bronchi inferiorly. The C-shaped cartilage ring provides essential mechanical support for the trachea to maintain its patency. Vascularized connective tissue not only tightly bind the C-shaped tracheal cartilage but also supplies the necessary nutrients for both cartilage and epithelium.[2] Recently, numerous studies have reported that three-dimensional (3D) printing techniques have shown significant potential for fabricating scaffolds that accurately mimic the anatomical structure of the natural trachea while also restoring the biological function of TETC.[3]

In our previous study, we utilized 3D printing techniques to fabricate C-shaped chondrocyte-laden GelMA hydrogel rings, which were subsequently vascularized *in vivo*, facilitating the development of TETC.[4] However, several crucial challenges remain to be addressed: (1) difficulty for the C-shaped chondrocyte-laden gelatin methacrylate (GelMA) hydrogel to retain its biomimetic C-type structure, primarily due to insufficient mechanical strength; (2) fusion of the regenerated C-shaped cartilage rings at a later stage due to the lack of a supporting structure to maintain the spacing between the C-shaped chondrocyte-laden GelMA hydrogel segments; and (3) restricted formation of vascularized connective tissue within the spacing between the C-shaped chondrocyte-laden GelMA hydrogel segments due to the lack of a regenerative scaffold. Thus, we propose to first 3D-print C-shaped PCL scaffolds and S-shaped PCL chains, followed by the incorporation of chondrocyte-laden GelMA and VEGF@GelMA hydrogels.

Numerous studies have reported the fabrication of TETC using 3D-printed scaffold.[5,6] Hsieh et al.[7] fabricated 3D-printed tubular scaffolds with elasticity and sufficient mechanical properties to replace a portion of the rabbit trachea *in vivo* without collapse. However, the tubular structure is unable to replicate the relaxation and contraction functions of natural C-shaped tracheal cartilage, nor is it conducive to the flexibility required for cervical tracheal bending.[8,9] Some researchers have further proposed a ring-based strategy, in which engineered cartilage rings and fiber-hydrogel rings are alternately stacked to form a tubular structure.[10,11] This approach results in a TETC with enhanced flexibility and improved nutrient supply.[12,13] However, Gao et al.[14] reported a 30% mortality rate in rabbits following reconstructive surgery, with even poorer outcomes observed in a goat model. This was primarily due to the absence of C-shaped cartilage rings, which are essential for regulating airflow velocity through their relaxation and contraction, aiding in the clearance of mucus from the lumen.[15]

Thus, we employed 3D printing techniques to fabricate a C-shaped polycaprolactone (PCL) scaffold and then filled the gaps with a chondrocyte-laden GelMA hydrogel to fabricate C-shaped chondrocyte-laden GelMA/PCL (CcGP) construct. The 3D-printed C-shaped PCL scaffold provides adequate mechanical support for the chondrocyte-laden GelMA hydrogel, helping it withstand *in situ* stress on the trachea until the C-shaped regenerated cartilage matures, thereby preserving its biomimetic structure. To address the issue of fusion between regenerated C-shaped cartilage rings at later stages, we introduced 3D-printed S-shaped PCL chains (SPC) to fix the CcGP construct. The S-shaped PCL chains effectively regulate the spacing between the regenerated C-shaped cartilages, preventing fusion of the cartilage rings in the later stages. The S-shaped PCL chains-C-shaped chondrocyte-laden GelMA/PCL (SPC-CcGP) construct also provides a sufficient and stable regenerative environment to promote the ingrowth of vascularized connective tissue into the gaps between CcGP constructs.

Prompt vascularization is crucial for the long-term survival of regenerated cartilage tissue and the functional performance of TETC within the trachea.[16] Our preliminary research demonstrated that placing regenerative scaffolds between cartilage rings not only creates a favorable environment for the regeneration of vascularized connective tissue but also accelerates the integration of various components within the regenerated trachea.[17,18] Vascular endothelial growth factor (VEGF) is widely recognized as a key pro-angiogenic growth factor, with extensive and well-established research supporting its role in vascular development.[19] Therefore, we utilized a silicone tube as the internal support for the SPC-CcGP construct, placing the entire assembly into a mold. The VEGF-loaded GelMA hydrogel was then poured into the gaps within the SPC-CcGP construct to fabricate TETC.

In summary, the current study introduces a novel strategy for constructing TETC by 3D printing techniques. First, the mechanical strength of the 3D-printed C-shaped PCL scaffold was continuously optimized through mechanical testing. Finite element analysis (FEA) was employed to characterize the deformation and displacement fields of the C-shaped cartilage rings under external force. Next, *in vitro* experiments were conducted to assess the growth of chondrocytes and human umbilical vein endothelial cells (HUVECs), while the regeneration of C-shaped cartilage was further evaluated *in vivo* through subcutaneous implantation in nude mice. Subsequently, TETC were

fabricated through mold casting and applied to repair a rabbit long-segment tracheal defect model instantly, with the efficacy of this repair strategy thoroughly evaluated. This study is expected to address key challenges associated with the deformation of 3D-printed C-shaped cell-laden hydrogels, the tendency for regenerated C-shaped cartilage to fuse, and the difficulty in regenerating vascularized connective tissue.

2. Materials and methods

2.1. Materials

PCL (Mn 80,000 g/mol, Sigma–Aldrich), trypsin, type II collagenase, phosphate-buffered saline (PBS), and fetal bovine serum (FBS) were purchased from Macklin (Shanghai Macklin Biochemical Co., Ltd., China). GelMA and lithium phenyl-2,4,6-trimethylbenzoyl-phosphinate (LAP) was purchased from EFL (Shanghai, China).

2.2. Three-dimensional printing of C-shaped PCL scaffolds and S-shaped PCL chains

The properties of C-shaped and S-shaped PCL frameworks were designed using Materialise Magics 22.0 software (Materialise HQ, Belgium), and the frameworks were printed using 3D bioprinter system (Regenovo 3D Bio-Architect). In brief, PCL (Mn 80 000 g/mol, Sigma–Aldrich) were melted (at 100°C) in a printing chamber and then printed with the following parameters: printing temperature of 80°C, speed of 40 mm/s, and nozzle diameter of 0.3 mm. The distance of the internal line was set to 1, 1.5, and 2 mm to obtain 1.0, 1.5, 2.0 mm C-shaped PCL scaffold, respectively. All frameworks were sterilized using ethylene oxide before use.

2.3. Characterizations of C-shaped PCL and GelMA/PCL scaffolds

First, the mechanical properties of 1.0, 1.5, 2.0 mm C-shaped PCL scaffold (n = 3) were analyzed using a mechanical testing machine (Instron-5542; Canton, USA). The samples from all groups were subjected to compression at a rate of 1 mm/min until the depth of compression reached 30% of the initial height. We computed the elastic modulus using the initial 5–15% of the strain–stress curve. Additionally, compressive forces were applied in various directions to a single PCL (1.5 mm), GelMA/PCL (1.5 mm), and natural tracheal cartilage until a 50% compression was achieved, with the maximum pressure recorded. The mechanical properties of identical length SPC-CcGP structures and natural trachea were further evaluated using the same methodology. Then, the volume of the gaps of the C-shaped PCL scaffold were conducted by evaluating the volume of hydrogel dropping into the scaffold (n = 3).

Furthermore, the enzymatic degradation of GelMA/PCL and PCL scaffolds were evaluated by using an enzymatic solution (0.05% w/v collagenase) for 96 h *in vitro*. Briefly, the initial mass of scaffolds was measured and recorded as M_0, respectively. Subsequently, scaffolds were put into the enzymatic solution at 37°C for degradation. The degraded scaffolds were taken out at time points 0, 8, 16, 24, 48, and 96 h, and then washed with distilled water. The scaffolds were dried at 60°C, and the weight of the degraded sample were measured and recorded as M_t. The remaining ratio was calculated as $(M_0 - M_t)/M_0 \times 100\%$ (n = 3).

The release kinetics of VEGF@GelMA were assessed as previously described. Briefly, the VEGF@GelMA hydrogel was immersed in PBS for varying durations. At designated time points, 500 μL of the medium was withdrawn, and an equivalent volume of fresh PBS was added to maintain the total volume. The quantity of VEGF released into the medium was determined using an ELISA Kit (R&D Systems, Minneapolis, MN, USA) according to the manufacturers instructions. The release kinetics were calculated using the following formula:

$$mt = m1+m2+m3+\ldots+mx$$

where mx represents the amount released at time x, and mt denotes the cumulative amount of released VEGF protein.

2.4. Chondrocyte's preparation

As previously reported, chondrocytes were isolated from auricular cartilage of New Zealand white rabbits (aged 2 months), purchased from Shanghai Jiagan Experimental Animal Raising Farm (Shanghai, China). Isolated chondrocytes were cultured in Dulbecco's modified Eagle's medium (DMEM) medium (Gibco BRL, Grand Island, NY, United States) containing 10% fetal bovine serum (FBS; Gibco BRL) and 1% antibiotic-antimycotic (Gibco BRL). Chondrocytes in passage 2 were harvested for use.

2.5. Bioactivity of GelMA/PCL on chondrocytes

For pristine GelMA hydrogel precursors, we dissolved 10% w/v GelMA and 0.3% w/v LAP (a photoinitiator) in PBS. Then, 8.0×10^6 cells/mL chondrocytes were mixed with 10% w/v GelMA hydrogel precursors and injected into PCL scaffold. The mixture was then polymerized using ultraviolet light irradiation (365 nm, 20 mW/cm^2) for 30 s to obtain chondrocyte-loaded hydrogels. Subsequently, chondrocyte-loaded hydrogels were incubated at 37°C and 5% CO_2 for 5 days. The culture medium (DMEM supplemented with 10% FBS and 1% antibiotic-antimycotic) was changed every 2 days. The viability of chondrocytes in hydrogels was assessed using a Live/Dead Cell Viability Assay kit (Invitrogen, USA) according to the manufacturer's instructions. Additionally, the samples were examined using a confocal microscope (Leica, TCS

SP8 STED 3X) on days 1, 3, and 5. The live/dead staining images were analyzed using the ImageJ software (Wayne Rasband and contributors National Institutes of Health, USA) to quantify cell viability. To observe cell spreading in the hydrogels on days 1, 3, and 5, F-actin and nuclei were stained with phalloidin (Yeasen Biotechnology, China) and DAPI, respectively. Thereafter, the samples were observed and photographed using a confocal microscope (Leica, TCS SP8 STED 3X). Cell proliferation was assessed via Cell Counting Kit-8 (CCK-8; Beyotime Biotechnology, China) assay and DNA quantification on days 1, 3, and 5. CCK-8 assay was performed according to the manufacturer's instructions, and absorbance was measured at 450 nm using a spectrophotometer. DNA was quantified using the PicoGreen dsDNA assay kit (Invitrogen, USA) according to the manufacturer's instructions.

2.6. Bioactivity of VEGF@GelMA on HUVECs

VEGF and 10% w/v GelMA hydrogel precursors were mixed together and polymerized using ultraviolet light irradiation (365 nm, 20 mW/cm^2) for 30 s to fabricate the VEGF@GelMA hydrogel. To assess the effect of VEGF@GelMA on the migration ability of HUVECs, 5×10^5 cells/well were seeded into a 6-well plate. After incubation at 37°C for 24 h, a scratch was made using a 10 μL pipette tip. Floating or dead cells were washed away with PBS. Furthermore, 500 μL VEGF@GelMA hydrogel was injected into 6 well plates, 500 μL GelMA was utilized as the control group. The remaining cells were cultured with different hydrogels for an additional 24 h. Cell migration was analyzed using ImageJ software. The average migration rate was calculated using the following formula:

$$\text{Migration rate} = (R_0 - R_1)/R_0 \times 100\% \quad \text{(II)}$$

where R_0 is an initial scratch area and R_1 is the unhealed scratch area.

An *in vitro* vessel formation assay was also conducted using Matrigel-coated plates. HUVECs (5×10^4 cells/well) were co-cultured with 100 μL different hydrogels in a 48-well plate for 6 h. The formation of capillary-like tubes was observed under a microscope and quantified using the ImageJ software. Specifically, the Angiogenesis Analyzer plugin in ImageJ was used to measure the number of branch points and the total capillary length within the vascular network.

To assess the gene expression levels of endothelial nitric oxide synthase (eNOS; *NOS3*), fibroblast growth factor 2 (FGF2; *FGF2*), and hypoxia-inducible factor-1α (HIF-1α; *HIF1A*), real-time polymerase chain reaction (RT-PCR) was performed. Briefly, HUVECs (2×10^4 cells/well) were seeded in a 48-well plate for 24 h, followed by treatment with different hydrogels for 48 h. Total RNA was extracted using the MolPure Cell/Tissue miRNA Kit (Yeasen Biotechnology, China), and reverse transcription was conducted with Hifair II 1st Strand cDNA Synthesis SuperMix (Yeasen Biotechnology, China). RT-PCR was used to quantify mRNA levels of *NOS3*, *FGF2*, and *HIF1A*, normalized to *GAPDH*. Relative mRNA expression was calculated using the $2^{-\Delta\Delta Ct}$ method. Primer sequences are provided in **Table S1** (Supporting Information).

In addition, the protein expression levels of eNOS, FGF2, and HIF-1α were detected via Western blotting. Briefly, total protein extractions were prepared from samples using RIPA buffer (KeyGen, China). Protein samples were separated by sodium dodecyl sulfate-polyacrylamide gel electrophoresis (SDS-PAGE), transferred onto polyvinylidene fluoride (PVDF) membranes, and blocked with 5% bovine serum albumin. Subsequently, the PVDF membranes were covered with primary antibodies as probes against eNOS, FGF2, and HIF-1α (1:1000; Santa Cruz Biotechnology, Inc.) and **β-actin** antibodies (1:10,000; Abcam). After applying horseradish peroxidase (HRP)-conjugated goat anti-rabbit/mouse IgG antibody (1:10,000; Aspen Biotech, Shanghai, China), band visualization was performed with the aid of the ECL kit (Aspen Biotech, Shanghai, China), and their intensity was analyzed using Band-Scan software (DEVA Broadcast Ltd., Bulgaria)

2.7. *In vitro* and *in vivo* CcGP regeneration

To fabricate CcGP construct, we homogeneously mixed chondrocytes in the pristine GelMA hydrogel precursors at a concentration of 1×10^8 cells/mL. The chondrocyte-loaded hydrogels were then loaded into C-shaped PCL scaffold and crosslinked via photopolymerization (365 nm, 20 mW/cm^2) for 30 s. Subsequently, CcGP constructs were cultured in a chondrogenic medium composed of DMEM, 10 ng/mL of transforming growth factor beta 1 (TGF-β1; R&D Systems Inc, USA), 40 ng/mL of dexamethasone (Sigma, USA), 100 ng/mL of insulin-like growth factor (IGF-1; R&D Systems Inc, USA), and other supplements for 6 weeks as described in a previous study.[14] Concurrently, the chondrocyte-loaded hydrogels were implanted into anesthetized nude mice (4-week-old male mice). The cartilage rings were harvested after 3 and 6 weeks of implantation.

2.8. *In vivo* biomimetic tracheal regeneration

Two 3D-printed SPC were used to fix the CcGP construct to create the SPC-CcGP construct. The SPC-CcGP construct was then placed into a mold. VEGF@GelMA hydrogel was poured into the gaps of the SPC-CcGP construct to generate TETC and crosslinked via photopolymerization (365 nm, 20 mW/cm^2) for 30 s. Subsequently, the 1.5-cm-long native trachea in rabbits was resected, and the defect

was orthotopically reconstructed using TETC promptly with intermittent sutures (5-0 monofilament, COVIDIEN). A 2-cm-long silicone tube was utilized as an internal support. After confirming the absence of air leak or bleeding, muscles and subcutaneous tissues were sutured, and the incision was closed. Furthermore, subcutaneous emphysema in the neck of the rabbit was observed at 6 h post-surgery to assess the presence of any gaps between the graft and the native trachea. Penicillin (50000 U, QD; Huachu, China) and meloxicam (0.1 mg/kg, QD; Xinan, China) were administered for the next 5 days. The rabbits were sacrificed at 3, 4, and 6 weeks after reconstruction. The orthotopically transplanted tracheas with 0.5-cm-long adjacent native tracheas were harvested. Gross view and endoscopic images were obtained.

2.9. Histological and biochemical evaluation

The above-mentioned samples were fixed in 4% paraformaldehyde for 24 h, embedded in paraffin and sectioned. Hematoxylin-eosin (H&E) staining was performed to evaluate the histological structure of the cartilage rings. Safranin-O staininh and immunohistochemical staining of collagen II were performed to analyze glycosaminoglycan (GAG) and type II collagen deposition. Masson's trichrome staining was performed as previously described[10] to observe collagen fibers. After H&E staining, blood vessels were counted under a 200× magnification field, with at least three random fields counted.

Simultaneously, samples were digested in papain (Sigma, USA), and total GAGs were precipitated using guanidinium chloride (GnCl). The GAG precipitate was dissolved, and the optical density (OD) was determined at 595 nm. Subsequently, GAG content was calculated based on a standard curve established using chondroitin-4-sulfate. Total collagen content was quantified via a hydroxyproline-based assay. Briefly, the samples were dissolved in an alkaline hydrolysis solution, and free hydroxyproline hydrolysates were quantified using a previously described method.

2.10. Statistical analysis

The results are presented as the mean ± standard deviation. Statistical analysis was performed using GraphPad Prism 9.5.0 (GraphPad Software, Inc., San Diego, CA, USA). Non-parametric *t*-tests were used to compare two groups at each time point. Values with $p < 0.05$ were considered statistically significant.

3. Results

3.1. Characterizations of C-shaped PCL and GelMA/PCL scaffolds

Customized 3D models for a C-shaped ring and SPC was designed (see Figure S1, Supporting Information). To optimize the distance of internal line of C-shaped PCL scaffold, the distance of the internal line was set to 1.0, 1.5, and 2 mm to 3D-print 1.0, 1.5, and 2.0 mm C-shaped PCL scaffold. The printed C-shaped PCL scaffold could maintain their original shape (Figure 2A1–A3). Moreover, Figure 2A1–A3 demonstrates that the pore size of the C-shaped PCL scaffold increased as the spacing between the internal lines widened. The pictures of side view of C-shaped PCL scaffold (Figure 2A4), SPC-CcGP construct (Figure 2A5), and TETC (Figure 2A6) are shown. We further evaluated the compressive strength and elastic modulus of C-shaped PCL scaffolds with 1.0, 1.5, and 2.0 mm. Compression tests revealed that the 1.0 mm scaffold exhibited the highest resistance to compression, followed by the 1.5 and 2.0 mm scaffolds (Figure 2B). Additionally, the elastic modulus for the 1.0, 1.5, and 2.0 mm scaffolds was measured as 23.001 ± 1.776, 18.739 ± 1.467, and 14.549 ± 1.185 kPa, respectively (Figure 2C). Figure 2D shows the volume for the 1.0, 1.5, and 2.0 mm scaffolds was 134 ± 10, 170 ± 3, and 241 ± 4 μL. Considering that the 1.5 mm C-shaped PCL scaffold demonstrated a balance of favorable mechanical properties and sufficient gap volume, it was selected for subsequent experiments. Figure 2E and F indicates that the maximum stress of both the single PCL (1.5 mm) and GelMA/PCL (1.5 mm) groups was greater than that of the single natural tracheal cartilage; however, no statistical significance was observed between the single PCL (1.5 mm) and GelMA/PCL (1.5 mm) groups. Additionally, Figure 2G and H demonstrates that the maximum force exerted by the SPC-CcGP construct in various directions is superior to that of natural trachea of the same length. Figure 2I demonstrates that the biodegradation rate of the GelMA/PCL scaffold was higher than that of the pure PCL scaffold, likely due to the faster degradation of the GelMA component within the composite structure. As shown in Figure 2J, the cumulative release of VEGF from the VEGF@GelMA hydrogel reached approximately 58.8% at 96 h, indicating that sustained release of VEGF can be achieved with the VEGF@GelMA hydrogel over this duration.

3.2. Bioactivity of GelMA/PCL on chondrocytes

Live/dead staining revealed that chondrocytes in both the GelMA/PCL and GelMA groups exhibited high viability with minimal cell death. Notably, the increase in green fluorescent signals over time may be attributed to the proliferation of chondrocytes in the GelMA (Figure 3B). F-actin/DAPI staining showed no significant differences in cell spreading between the GelMA/PCL and GelMA groups on days 1, 3, and 5 (Figure 3B). These observations were further confirmed by quantitative analysis of cell viability (Figure 3C) and CCK8 (Figure 3D). The results of DNA quantification indicated that there was no statistically significant difference in cell proliferation between the GelMA/PCL and GelMA groups on days 1, 3, and 5 (Figure 3E).

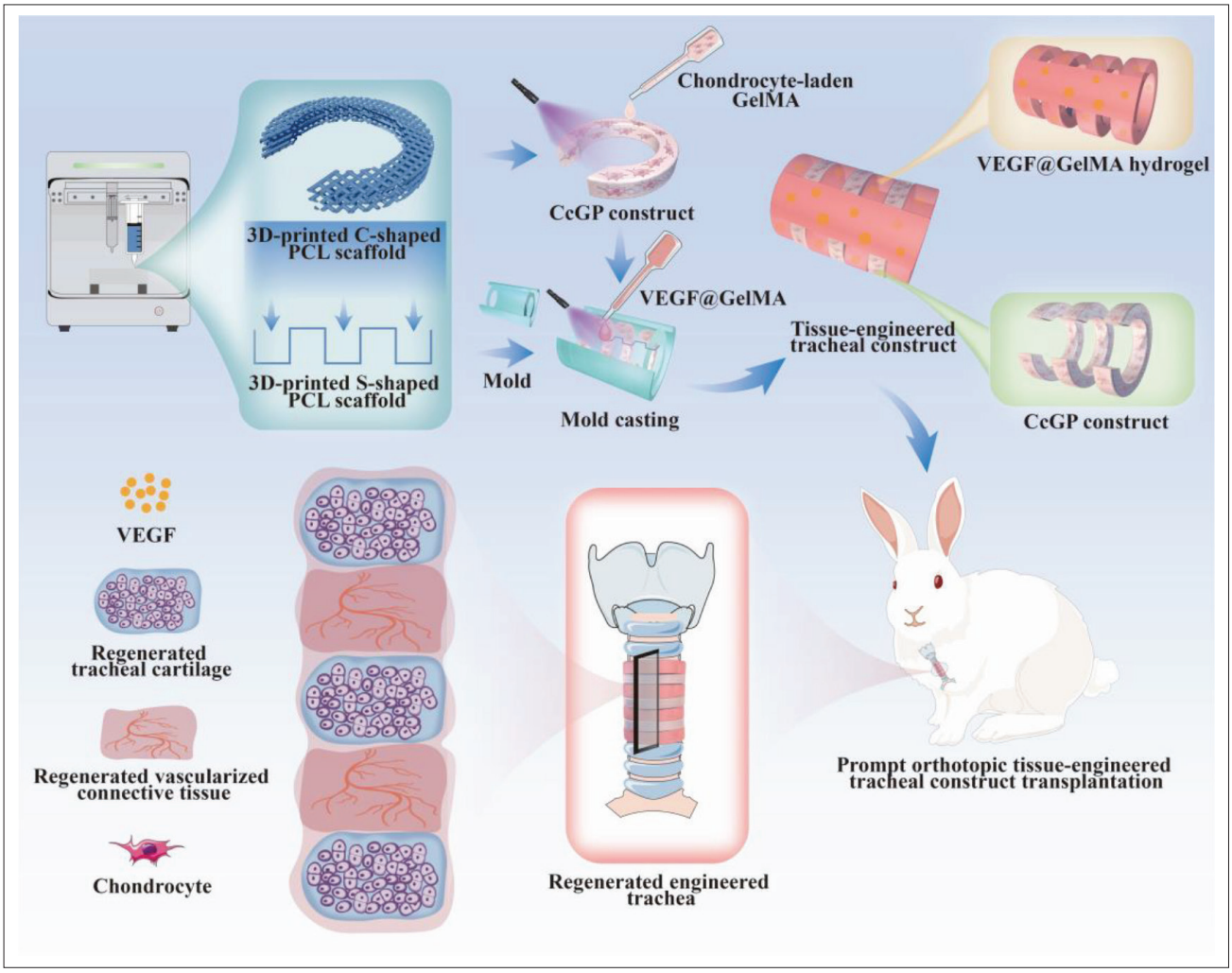

Figure 1. Schematic diagram of the overall experiments. First, C-shaped PCL scaffolds and S-shaped PCL chains were fabricated using 3D printing technology. Next, the chondrocyte-laden GelMA hydrogel was introduced into the gaps of the C-shaped PCL scaffold and crosslinked via photopolymerization to form the C-shaped chondrocyte-laden GelMA/PCL (CcGP) construct. The CcGP construct was then integrated into the S-shaped PCL chains (SPC) to create the SPC-CcGP construct. Subsequently, the SPC-CcGP construct was placed into a mold, and VEGF@GelMA hydrogel was poured into the gaps to generate the tissue-engineered tracheal construct (TETC). Finally, the TETC was used to regenerate biomimetic trachea in a rabbit model with a long-segment tracheal defect. Abbreviations: CcGP, C-shaped chondrocyte-laden GelMA/PCL; GelMA, gelatin methacrylate; PCL, polycaprolactone; VEGF, vascular endothelial growth factor.

3.3. Bioactivity of VEGF@GelMA hydrogel on HUVECs

Cell migration was assessed using a cell scratch assay. Results showed that the VEGF@GelMA group (75.44 ± 4.99%) exhibited enhanced cellular migration of HUVECs compared to GelMA group (40.60 ± 3.40%) (Figure 4A and B). Additionally, the tube formation assay demonstrated the same trend. Figure 4C revealed that the VEGF@GelMA group displayed a significantly higher number of tubes and increased tube length compared to GelMA group. The quantitative results presented consistent trends (Figure 4D and E). Compared with the GelMA group, the quantitative RT-PCR results for the VEGF@GelMA group showed higher expression of angiogenic genes, including *NOS3*, *FGF2*, and *HIF1A* (Figure 4F–H). In addition, Western blot results also showed higher protein expressions of eNOS, FGF2, and HIF-1α in VEGF@GelMA group compared with GelMA group (Figure S2, Supporting Information). These findings highlighted the enhanced angiogenic potential of VEGF@GelMA hydrogel, indicating its suitability for promoting angiogenesis and tissue regeneration applications.

3.4. Cartilage regeneration of CcGP construct *in vitro* and *in vivo*

To assess the cartilage regeneration ability of CcGP construct, C-shaped cartilage rings were regenerated and evaluated *in vitro* (Figure 5A). After 3 weeks of

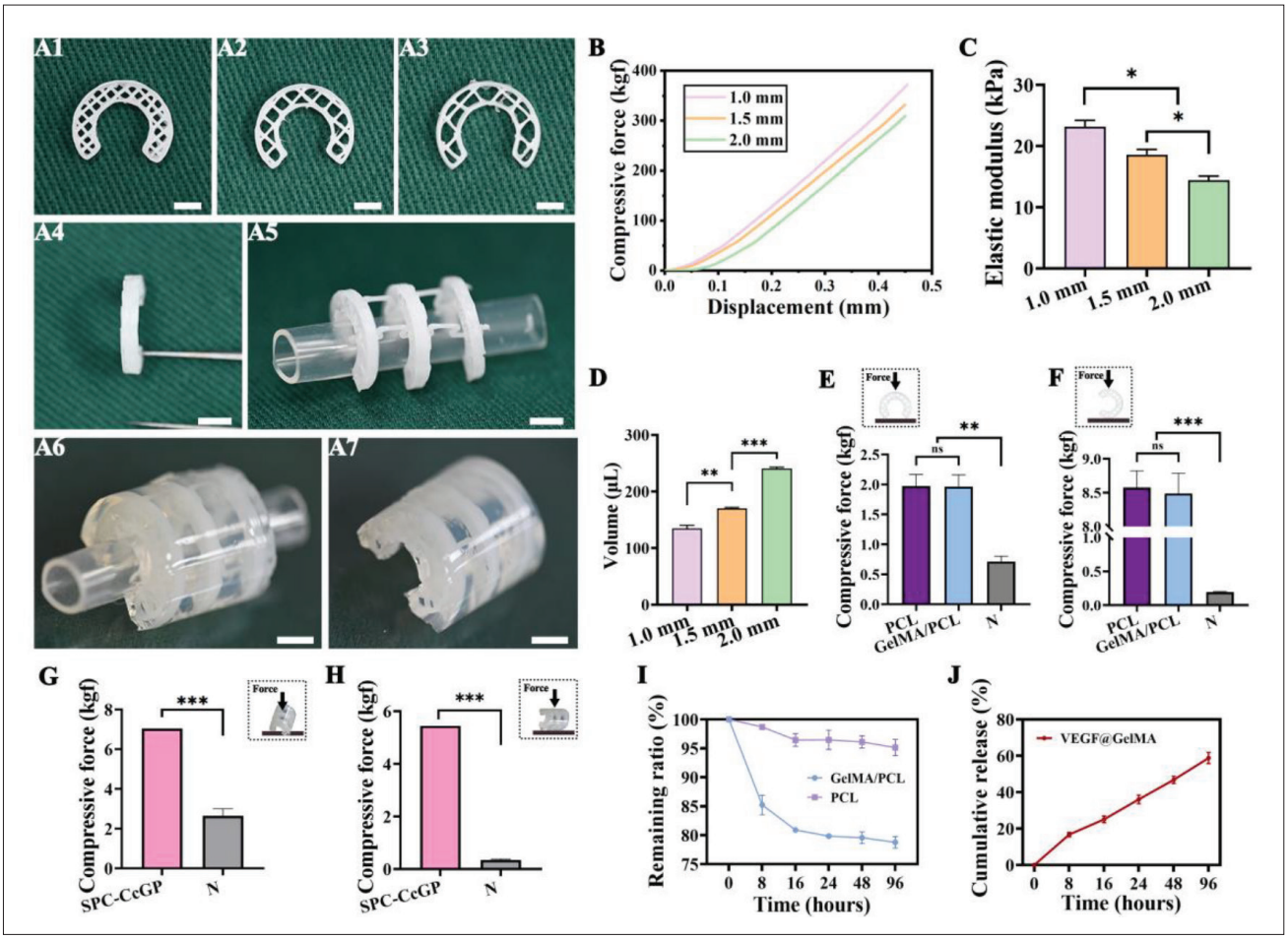

Figure 2. Characterizations of the 3D-printed C-shaped GelMA/PCL and PCL scaffolds. (A1–A3) 3D-printed 1.0 mm (A1), 1.5 mm (A2), and 2.0 mm (A3) PCL scaffolds in C shape. (A4) Side view of C-shaped PCL scaffold. (A5–A7) Fabrication of SPC-CcGP construct (A5) and TETC (A6, A7) with the assistance of a silicone tube. Scale bars: 3 mm. (B) Compressive force and (C) elastic modulus of 1.0, 1.5, and 2.0 mm C-shaped PCL scaffolds. (D) The volume of the gaps of the C-shaped PCL scaffold. (E, F) Compressive forces applied in various directions on the single PCL, GelMA/PCL, and natural tracheal cartilage (N). (G, H) Compressive forces applied in various directions on the SPC-CcGP construct and natural trachea (N). (I) *In vitro* biodegradability of GelMA/PCL and pure PCL scaffold. (J) Cumulative release kinetics of VEGF from the VEGF@GelMA hydrogel. $*p < 0.05$, $**p < 0.01$, $***p < 0.001$. Abbreviations: CcGP, C-shaped chondrocyte-laden GelMA/PCL; GelMA, Gelatin methacrylate; N, natural tracheal tissue/natural trachea; PCL, polycaprolactone; SPC, S-shaped PCL chains.

chondrogenic culture *in vitro*, H&E staining revealed that CcGP construct could form prominent cartilage-specific lacunae. The results of safranin-O, collagen II, and Masson's trichrome staining indicated that regenerated cartilage of CcGP construct had cartilage-specific extracellular matrix (ECM) deposition (Figure 5B). The cartilage-regenerating ability of CcGP construct was further evaluated in nude mice (Figure 5C). Figure 5D shows the intact C-shaped geometry of regenerated C-shaped cartilage rings. The H&E staining revealed that the regenerated cartilage of CcGP construct developed typical lacunae, and a homogeneous structure was observed at 3 weeks. The intense and homogeneous staining of safranin-O, collagen II, and Masson's trichrome indicated that cartilage-specific ECM deposition formed after 3 weeks cultivation in nude mice (Figure 5D). Furthermore, GAG content and total collagen content validated that the regenerated cartilage of CcGP construct matured with prolonged *in vitro* (Figure 5E and F) and *in vivo* (Figure 5G and H) incubation.

3.5. Regeneration of cartilage and vascularized connective tissue after prompt orthotopic transplantation of trachea

A long segmental tracheal defect in rabbit model was established (Figure S3A–B, Supporting Information), and the TETC was used to orthotopically reconstruct this tracheal defect (Figure S3C, Supporting Information). The gross and endoscopic images in Figure 6A demonstrate that the regenerated engineered tracheal tissue maintained an unobstructed lumen for 3 weeks, with no evidence of

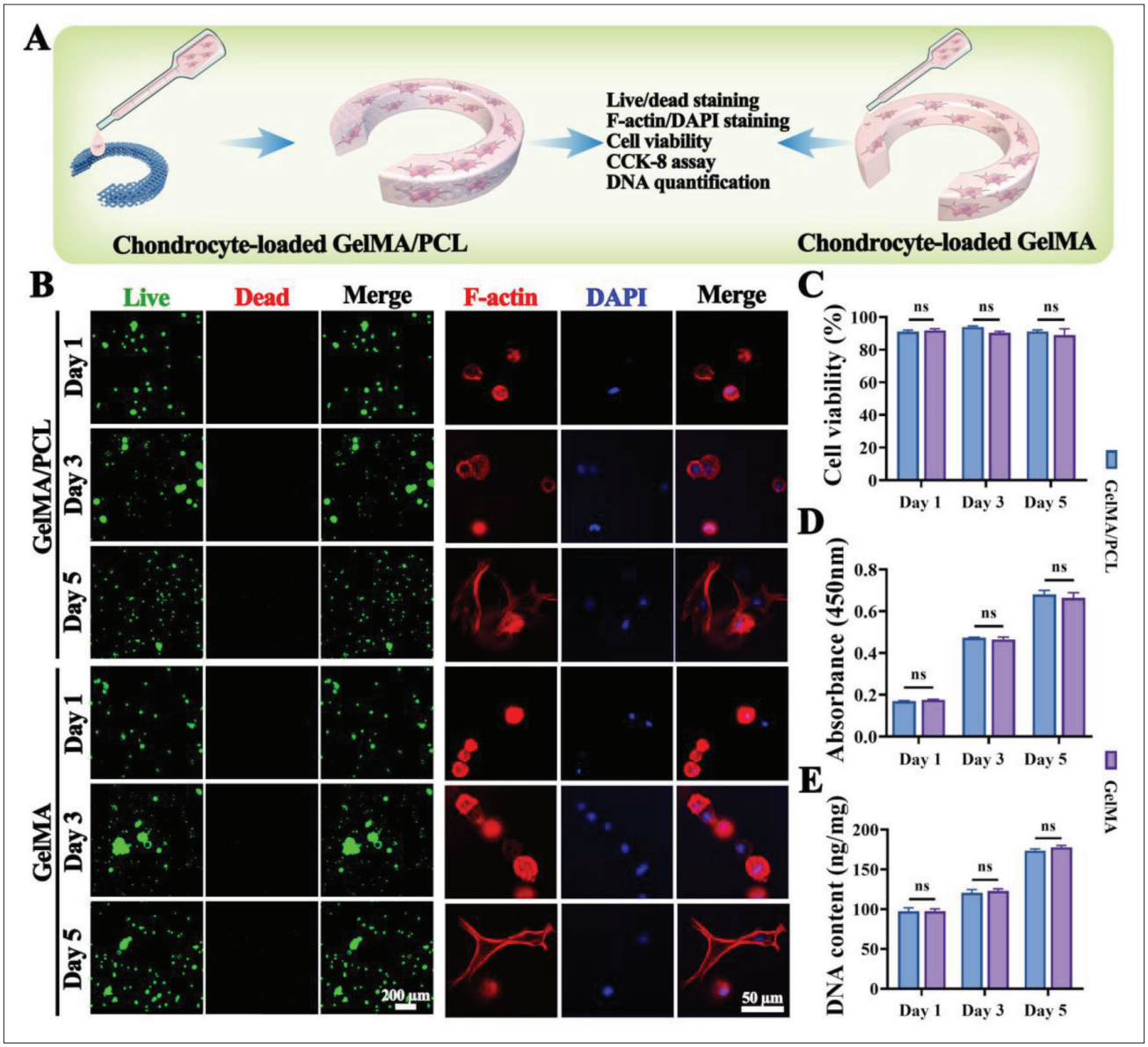

Figure 3. Bioactivity of GelMA/PCL and pure GelMA hydrogel on chondrocytes. (A) Schematic representation of chondrocyte-loaded GelMA/PCL and GelMA hydrogel. (B) Live/dead and F-actin/DAPI staining of chondrocytes in GelMA/PCL and pure GelMA. (C–E) Results on cell viability (C), cell proliferation based on CCK-8 assay (D) and DNA quantification (E) in chondrocyte-loaded GelMA/PCL and GelMA hydrogels on days 1, 3, and 5. Abbreviations: GelMA, gelatin methacrylate; ns, no statistical significance; PCL, polycaprolactone.

airway obstruction. The vertical and sectional views of the orthotopically regenerated engineered tracheal tissue after 4 and 6 weeks indicate the integration of tubular structure (Figure S4A–B, Supporting Information), suggesting that the mechanical strength of the engineered trachea is sufficient to preserve lumen patency. Besides, through repeated application of force to the implanted bioengineered trachea, we observed that the bioengineered trachea effectively maintained the shape of the lumen without causing obstruction (Video S1, Supporting Information). Furthermore, the experimental animals exhibited no signs of coughing, wheezing, or shortness of breath. Figure 6B shows schematic representation of the orthotopically regenerated engineered tracheal tissue. Compared to wide inner-diameter blood vessels of native trachea (Figure 6C), the regenerated engineered tracheal tissue exhibited a smaller lumen but a higher density of neovascularization (Figure 6D). Quantitative analysis showed that the VEGF/GelMA group promoted significantly more neovascularization compared to GelMA alone (Figure 6E).

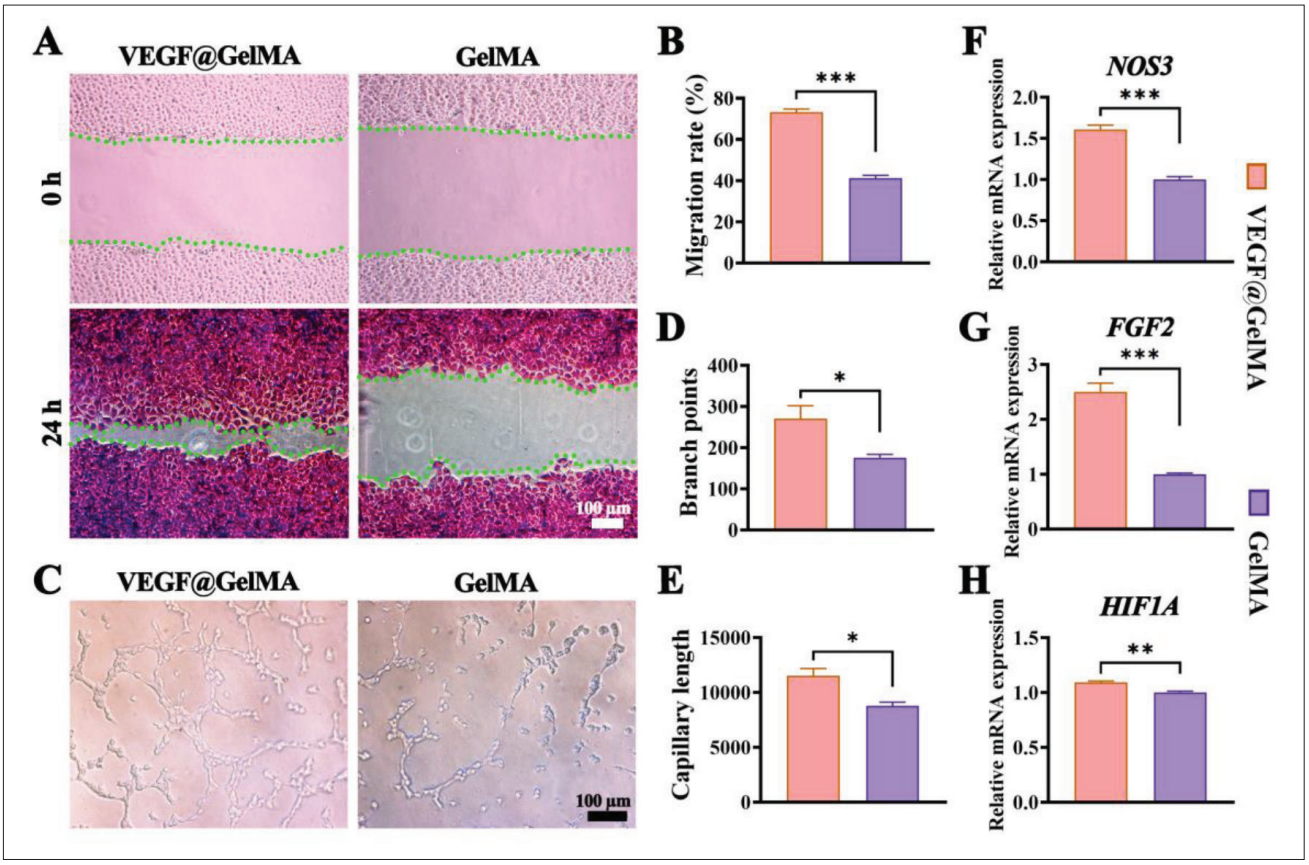

Figure 4. Angiogenic evaluation of VEGF@GelMA and pure GelMA hydrogel on HUVECs. (A, B) HUVEC migration ability as determined by cell scratch assay (A) and the corresponding quantitative outcomes (B). (C–E) Results of tube formation assay (C) and the quantitative outcomes regarding branch point number (D) and capillary length (E) of HUVECs. (F–H) Expression levels of key angiogenesis-related genes in HUVECs. *$p < 0.05$, **$p < 0.01$, ***$p < 0.001$. Abbreviations: GelMA, gelatin methacrylate; VEGF, vascular endothelial growth factor.

Masson's trichrome staining demonstrated that the regenerated C-shaped cartilage rings maintained their geometry 3 weeks after orthotopic transplantation. H&E staining revealed the formation of prominent cartilage-specific lacunae in the regenerated tracheal cartilage. Additionally, Safranin-O staining indicated the presence of cartilage-specific ECM deposition after 3 weeks (Figure 6F). Quantitative analysis further revealed that GAG content and total collagen content in the regenerated tracheal cartilage increased at 6 weeks compared to 3 weeks (Figure 6G and H). These findings confirmed that the TETC effectively repair tracheal defects, maintain lumen patency, and promote both neovascularization and cartilage regeneration.

4. Discussion

Currently, a strategy of direct excision and end-to-end anastomosis of the trachea is not feasible in adult patients, when more than half of the airway is affected.[20] Tracheal tissue engineering offers promising potential to address this clinical challenge. Several tracheal replacement strategies have been developed, including intact cartilaginous tubes and assembled constructs featuring either interrupted O-shaped or C-shaped cartilage rings.[21] However, these approaches faced challenges, such as the deformation of 3D-printed C-shaped cell-laden hydrogels, the tendency of regenerated C-shaped cartilage to fuse, and the difficulty in regenerating vascularized connective tissue.

Emerging 3D extrusion bioprinting strategies based on photocrosslinkable hydrogels have proven to be an attractive technology for the construction of heterogeneous tissue architectures.[22] Our preliminary research demonstrated that 3D printing of cell-laden photocrosslinked hydrogels allowed for precise shape control in order to mimic tracheal tissue. However, regenerating biomimetic tracheal tissue *in vivo* often resulted in deformation due to compression from surrounding tissues.[4] We hypothesized that this deformation was likely caused by the insufficient mechanical strength of the hydrogel, restraining immediate and effective tracheal reconstruction. Additionally, regenerating engineered trachea typically

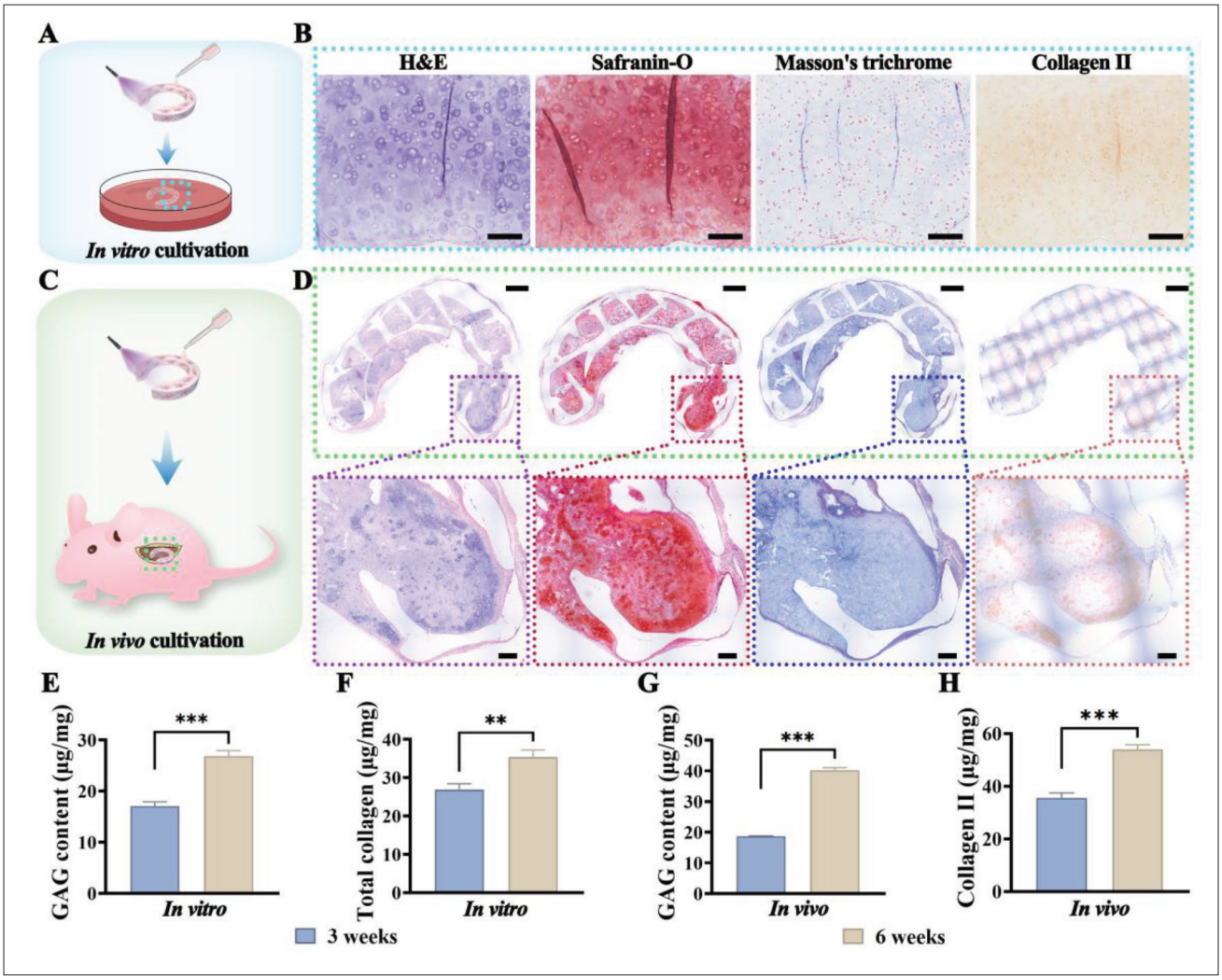

Figure 5. Cartilage regeneration of CcGP construct after *in vitro* and *in vivo* cultivation. (A) Schematic representation of *in vitro* regeneration of cartilage using chondrocyte-loaded GelMA hydrogel (blue dotted box indicates the regenerated cartilage *in vitro*). (B) Representative images of H&E, Safranin-O, Masson's trichrome, immunohistochemical collagen II staining of chondrocyte-loaded GelMA hydrogel after 3 weeks of *in vitro* chondrogenic culture. Scale bar: 200 μm. (C) Schematic representation of *in vivo* regeneration of C-shaped cartilage using CcGP construct (green-dotted box indicates the regenerated cartilage *in vivo*). (D) Representative images of H&E, Safranin-O, Masson's trichrome, immunohistochemical collagen II staining of chondrocyte-loaded GelMA hydrogel after 3 weeks in nude mice. Scale bar: 2 mm (main); 500 μm (inset). (E–H) Contents of GAG and collagen II, *in vitro* and *in vivo*, at 3 and 6 weeks. $^{**}p < 0.01$, $^{***}p < 0.001$. Abbreviations: CcGP, C-shaped chondrocyte-laden GelMA/PCL; GAG, Glycosaminoglycan; H&E, Hematoxylin-eosin.

requires a two-stage approach, involving intramuscular pre-implantation followed by end-to-end anastomosis through pedicled muscle transplantation, which is an intricate and time-consuming operation.[23] Researchers have explored the use of 3D bioprinted C-shaped TETCs for direct end-to-end anastomosis to repair segmental defects in the rabbit trachea, highlighting the potential of advanced 3D bioprinting for rapid and effective tracheal reconstruction.[5] Nevertheless, simply constructing TETCs with cell-laden hydrogels often lacks sufficient mechanical strength in the early stages of regeneration, necessitating internal support to maintain lumen patency.[5] Further, a "concrete-rebar structure" has been proposed as a strategy for tracheal tissue engineering. In this approach, bioengineered cartilage rings are fabricated by 3D-printing PCL combined with rabbit chondrocytes, while transmural angiogenesis is promoted by incorporating 3D printing PCL fibers and GelMA. Although this method offers early mechanical support for TETC, it involves an intricate and time-consuming operation to achieve full reconstruction.[13]

Here, we utilized a chondrocyte-laden GelMA and VEGF@GelMA hydrogel approach to simplify the

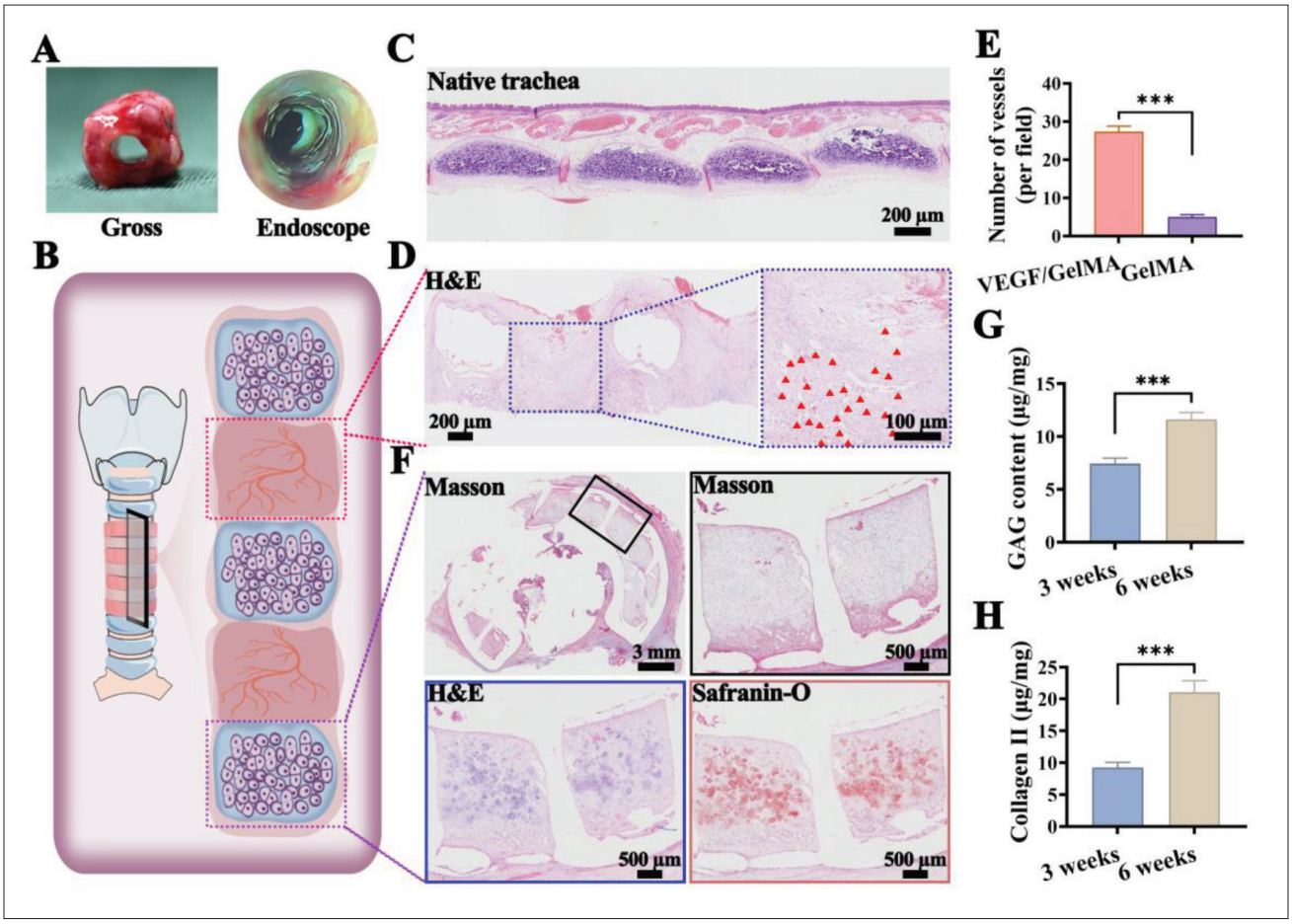

Figure 6. Prompt repair of tracheal defects using TETC in a rabbit model. (A) Gross view and endoscopic images at 3 weeks of regenerating engineered tracheal tissue. (B) Schematic representation of orthotopic regeneration of engineered tracheal tissue (red-dotted box indicates the regenerated vascularized connective tissue, whereas purple-dotted box indicates the regenerated cartilage). (C, D) H&E staining of native trachea (C) and regenerated vascularized connective tissue (D) after orthotopic tracheal transplantation at 3 weeks. (E) Number of vessels per field in VEGF/GelMA and GelMA hydrogels. (F) Masson's trichrome, H&E, safranin-O staining of regenerated tracheal tissue after orthotopic tracheal transplantation at 3 weeks. (G, H) GAG content (G) and collagen II content (H) at 3 and 6 weeks.***p <0.001. Abbreviations: GAG, glycosaminoglycan; GelMA, gelatin methacrylate; H&E, Hematoxylin-eosin; TETC, tissue-engineered tracheal construct; VEGF, vascular endothelial growth factor.

preparation process of TETC. The CcGP construct provided essential mechanical support to the engineered trachea, maintaining an unobstructed lumen and preventing cartilage deformation under compressive forces. The incorporation of SPC effectively maintained the spacing between the engineered tracheal cartilage, preventing fusion of the regenerated C-shaped cartilage and allowing space for the ingrowth of connective tissue. Blood vessels play a crucial role in wound healing and tissue regeneration, and vessel ingrowth from the host tissues into the TETC is vital for supplying adequate nutrients to the regenerated cartilage during tracheal defect reconstruction.[24,25] To facilitate this, we filled the gaps in the SPC-CcGP construct with VEGF@GelMA hydrogel to construct the TETC with sufficient mechanical strength and effective vascular regeneration for timely tracheal defect repair.

VEGF is a critical regulator of angiogenesis, the process of new blood vessel formation. It facilitates endothelial cell proliferation, migration, and differentiation, leading to capillary development and increased vascular permeability. This function is essential for providing an adequate supply of nutrients and oxygen to cartilage, particularly during regeneration.[26] Furthermore, VEGF has been demonstrated to enhance chondrocyte proliferation and promote the synthesis of cartilage-specific ECM components, such as collagen and proteoglycans.[27] The establishment of a vascular network is vital for meeting the metabolic demands of regenerating cartilage, thereby contributing to its structural integrity and overall functionality.

Our *in vitro* results demonstrated that the C-shaped PCL scaffold possesses sufficient mechanical properties

and biocompatibility, as evidenced by subcutaneous cartilage regeneration in nude mice. Additionally, *in vitro* experiments confirmed that VEGF@GelMA hydrogel effectively promotes angiogenesis. We selected PCL and GelMA for scaffold fabrication due to its excellent biodegradability and biocompatibility.[28,29] We speculated that the regenerated tracheal cartilage will progressively exhibit the mechanical support role of the C-shaped PCL scaffold with the degradation of PCL and GelMA. Furthermore, the formation of vascularized connective tissue will tightly bind the regenerated C-shaped tracheal cartilage, facilitating the successful regeneration of the engineered trachea.

Even though TETC can achieve stable regeneration of cartilage and vascularized connective tissue, as well as maintain luminal patency, it still has a certain limitation: a longer experimental period is needed to further verify the relationship between PCL degradation and the regeneration of cartilage tissue and vascularized connective tissue. Further evaluation of infection and inflammation indexes is necessary to assess their impact on TETC outcomes.

5. Conclusion

In this study, we initially utilized a 3D-printed C-shaped PCL scaffold to provide early mechanical support for the regenerated engineered trachea. Subsequently, mold casting was applied to construct TETC, which could effectively promote the regeneration of interspersed cartilage and vascularized connective tissue simultaneously. This strategy is expected to offer a promising strategy for prompt tracheal defect repair.

Acknowledgments

None.

Funding

The research was supported by the National Natural Science Foundation of China (82300068, 82102227, and 82302395), Young Elite Scientists Sponsorship Program by CAST (2023QNRC001), and the Natural Science Foundation of Shanghai (22YF1437400).

Conflict of interest

The authors declare that they have no conflicts of interest.

Author contributions

Conceptualization: Pengli Wang
Formal analysis: Lei Xie
Investigation: Ziming Wang
Methodology: Bohui Li
Writing–original draft: Liang Guo and Yong Xu
Writing–review & editing: Dan Li, Jiaoyu Yi and Tao Bo

Ethics approval and consent to participate

All animal experiments were performed in accordance with the Guide for the Care and Use of Laboratory Animals guidelines and were approved by the Shanghai Pulmonary Hospital Ethics Committee (K21-355Y).

Consent for publication

Not applicable.

Availability of data

The data that support the findings of this study are available from the corresponding author upon reasonable request.

References

1. Wei S, Zhang Y, Luo F, et al. Tissue-engineered tracheal implants: advancements, challenges, and clinical considerations. *Bioeng Transl Med*. 2024;9(4):e10671. doi: 10.1002/btm2.10671
2. Furlow PW, Mathisen DJ. Surgical anatomy of the trachea. *Ann Cardiothorac Surg*. 2018;7(2): 255-260. doi: 10.21037/acs.2018.03.01
3. Matai I, Kaur G, Seyedsalehi A, McClinton A, Laurencin CT. Progress in 3D bioprinting technology for tissue/organ regenerative engineering. *Biomaterials*. 2020;226:119536. doi: 10.1016/j.biomaterials.2019.119536
4. Wang P, Wang T, Xu Y, Song N, Zhang X. 3D-bioprinted cell-laden hydrogel with anti-inflammatory and anti-bacterial activities for tracheal cartilage regeneration and restoration. *IJB*. 2023;10(1):0146. doi: 10.36922/ijb.0146
5. Sun Y, Huo Y, Ran X, et al. Instant trachea reconstruction using 3D-bioprinted C-shape biomimetic trachea based on tissue-specific matrix hydrogels. *Bioact Mater*. 2024;32:52-65. doi: 10.1016/j.bioactmat.2023.09.011
6. Song X, Zhang P, Luo B, et al. Multi-tissue integrated tissue-engineered trachea regeneration based on 3D printed bioelastomer scaffolds. *Adv Sci*. 2024;11(39):e2405420. doi: 10.1002/advs.202405420
7. Hsieh C.-T., Liao C.-Y., Dai N.-T., et al. 3D printing of tubular scaffolds with elasticity and complex structure from multiple waterborne polyurethanes for tracheal tissue engineering. *Appl Mater Today*. 2018;12:330-341. doi: 10.1016/j.apmt.2018.06.004
8. Park JH, Ahn M, Park SH, et al. 3D bioprinting of a trachea-mimetic cellular construct of a clinically relevant size. *Biomaterials*. 2021;279:121246. doi: 10.1016/j.biomaterials.2021.121246

9. Park JH, Park JY, Nam I-C, et al. A rational tissue engineering strategy based on three-dimensional (3D) printing for extensive circumferential tracheal reconstruction. *Biomaterials*. 2018;185: 276-283. doi: 10.1016/j.biomaterials.2018.09.031

10. Xu Y, Guo Y, Li Y, et al. Biomimetic trachea regeneration using a modular ring strategy based on poly(sebacoyl diglyceride)/polycaprolactone for segmental trachea defect repair. *Adv Funct Mater*. 2020;30(42):2004276. doi: 10.1002/adfm.202004276

11. Xu Y, Dai J, Zhu X, et al. Biomimetic trachea engineering via a modular ring strategy based on bone-marrow stem cells and atelocollagen for use in extensive tracheal reconstruction. *Adv Mater*. 2022;34(6):2106755. doi: 10.1002/adma.202106755

12. Park JH, Hong JM, Ju YM, et al. A novel tissue-engineered trachea with a mechanical behavior similar to native trachea. *Biomaterials*. 2015;62:106-115. doi: 10.1016/j.biomaterials.2015.05.008.

13. Tang H, Sun W, Liu X, et al. A bioengineered trachea-like structure improves survival in a rabbit tracheal defect model. *Sci Transl Med*. 2023;15(714):eabo4272. doi: 10.1126/scitranslmed.abo4272

14. Gao E, Wang Y, Wang P, et al. C-shaped cartilage development using Wharton's Jelly-derived hydrogels to assemble a highly biomimetic neotrachea for use in circumferential tracheal reconstruction. *Adv Funct Mater*. 2023;33(14):2212830. doi: 10.1002/adfm.202212830

15. Luo X, Liu Y, Zhang Z, et al. Long-term functional reconstruction of segmental tracheal defect by pedicled tissue-engineered trachea in rabbits. *Biomaterials*. 2013; 34(13): 3336-3344. doi: 10.1016/j.biomaterials.2013.01.060

16. Li D, Yin Z, Liu Y, et al. Regeneration of trachea graft with cartilage support, vascularization, and epithelization. *Acta Biomater*. 2019;89: 206-216. doi: 10.1016/j.actbio.2019.03.003

17. Xu Y, Duan L, Li Y, et al. Nanofibrillar decellularized Wharton's Jelly matrix for segmental tracheal repair. *Adv Funct Mater*. 2020;30(14):1910067. doi: 10.1002/adfm.201910067

18. Gao E, Li G, Cao R, et al. Bionic tracheal tissue regeneration using a ring-shaped scaffold comprised of decellularized cartilaginous matrix and silk fibroin. *Compos B: Eng*. 2022;229:109470. doi: 10.1016/j.compositesb.2021.109470

19. Xu W, Wu Y, Lu H, et al. Sustained delivery of vascular endothelial growth factor mediated by bioactive methacrylic anhydride hydrogel accelerates peripheral nerve regeneration after crush injury. *Neural Regen Res*. 2022;17(9):2064-2071. doi: 10.4103/1673-5374.335166

20. Dikina AD, Alt DS, Herberg S, et al. A modular strategy to engineer complex tissues and organs. *Adv Sci (Weinh)*. 2018;5(5):1700402. doi: 10.1002/advs.201700402

21. Damiano G, Palumbo VD, Fazzotta S, et al. Current strategies for tracheal replacement: a review. *Life (Basel)*. 2021;11(7):618. doi: 10.3390/life11070618

22. Zhang YS, Haghiashtiani G, Hübscher T, et al. 3D extrusion bioprinting. *Nat Rev Methods Primers*. 2021;1(1):75. doi: 10.1038/s43586-021-00073-8

23. Xu Y, Li D, Yin Z, et al. Tissue-engineered trachea regeneration using decellularized trachea matrix treated with laser micropore technique. *Acta Biomater*. 2017;58:113-121. doi: 10.1016/j.actbio.2017.05.010

24. Crowley C, Klanrit P, Butler CR, et al. Surface modification of a POSS-nanocomposite material to enhance cellular integration of a synthetic bioscaffold. *Biomaterials*. 2016; 83:283-293. doi: 10.1016/j.biomaterials.2016.01.005

25. Eming SA, Martin P, Tomic-Canic M. Wound repair and regeneration: mechanisms, signaling, and translation. *Sci Transl Med*. 2014;6(265):265sr6. doi: 10.1126/scitranslmed.3009337

26. Hu K, Olsen BR. Vascular endothelial growth factor control mechanisms in skeletal growth and repair. *Dev Dyn*. 2017;246(4):227-234. doi: 10.1002/dvdy.24463

27. Li M, Yin H, Yan Z, et al. The immune microenvironment in cartilage injury and repair. *Acta Biomater*. 2022;140:23-42. doi: 10.1016/j.actbio.2021.12.006

28. Li X, Cho B, Martin R, et al. Nanofiber-hydrogel composite–mediated angiogenesis for soft tissue reconstruction. *Sci Transl Med*. 2019;11(490):eaau6210. doi: 10.1126/scitranslmed.aau6210

29. Liu Y, Zheng K, Meng Z, et al. A cell-free tissue-engineered tracheal substitute with sequential cytokine release maintained airway opening in a rabbit tracheal full circumferential defect model. *Biomaterials*. 2023;300:122208. doi: 10.1016/j.biomaterials.2023.122208